Ultrasonics - Sonochemistry 44 (2018) 1–13

Contents lists available at ScienceDirect

Ultrasonics - Sonochemistry

journal homepage: www.elsevier.com/locate/ultson

Sono-synthesis approach in uniform loading of ultrafine Ag nanoparticles on reduced graphene oxide nanosheets: An efficient catalyst for the reduction of 4-Nitrophenol

Zahra Mohammadi[a], Mohammad H. Entezari[a,b,*]

[a] Sonochemical Research Center, Department of Chemistry, Faculty of Science, Ferdowsi University of Mashhad, 91779 Mashhad, Iran
[b] Environmental Chemistry Research Center, Department of Chemistry, Faculty of Science, Ferdowsi University of Mashhad, 91779 Mashhad, Iran

ARTICLE INFO

Keywords:
Ultrasound
Reduced graphene oxide/Ag nanocomposite
Polyol
4-Nitrophenol

ABSTRACT

In this research, a facile, one step and eco-friendly sonochemical rout was utilized to the synthesis of a new nanocomposite by Ag nanoparticle anchored on reduced graphene oxide (rGO-Ag-U). Sonication was carried out by using low frequency ultrasound (20 kHz) under ambient condition. In this way, graphene oxide and Ag^+ ions simultaneously reduced by polyol without using any additional reactants or capping agents. The polyol serves as both solvent and low toxic reducing agent. To achieve the best synthesis condition of rGO-Ag-U nanocomposite, the effects of irradiation time, ultrasonic amplitude and reaction temperature were investigated. In comparison, the synthesis of rGO-Ag was also carried out via reflux as a classical method (rGO-Ag-C). It was found that ultrasonic irradiation for 10 min at 70% amplitude was sufficient for the synthesis of rGO-Ag-U. Several analytical techniques were used to characterize the resulting nanocomposites such as UV–Vis spectroscopy, Fourier transform infrared spectroscopy (FT-IR), X-ray diffraction (XRD) and transmission electron microscopy (TEM). The UV–Vis spectra show a shift of GO band to a higher wavelength which is due to the reduction of sp^3 sites. The results of TEM also confirm the smaller Ag nanoparticle (about 18 nm) which uniformly decorated on rGO nanosheets by sonochemical method than classical method. The experimental data suggest that among the synthesized nanocomposites, rGO-Ag-U exhibited better catalytic activity (k_{app} = 1.18 min^{-1}) towards the reduction of 4-Nitrophenol to 4-Aminophenol in the presence of sodium borohydride ($NaBH_4$).

1. Introduction

Graphene is a two-dimensional (2D) carbon material [1] that has rapidly become known as perfect candidate for application in various fields due to its unique properties such as mechanical, electrical, chemical, thermal, and optical properties [2–4]. Since its discovery in 2004, a lot of synthetic strategies have been developed, e.g. micromechanical exfoliation of graphite, chemical vapor deposition, epitaxial growth and solution-based chemical reduction of graphene oxide (GO) to reduced graphene oxide (rGO) [5,6]. Among these, the chemical reduction of GO to rGO is the most suitable and efficient route owing to its low cost and facile synthetic nature in a controlled, scalable, and reproducible manner. However, as-prepared reduced graphene sheets tend to form irreversible agglomerates or even restack to form graphite due to the van der Waals interactions [7]. Hence, researchers look for versatile methods to overcome the above shortcomings for obtaining non-agglomerated graphene.

Over the years, metal particles at nanolevel dimensional have attracted increasing attention because of their exclusive electronic, optical, magnetic and catalytic properties, which are totally different from those of bulk metals. These nanoparticles have been shown remarkable potential for numerous applications in electronic, chemical, biological, and medical fields and so on [8–11]. However, metal nanoparticles with small size are not at a thermodynamic stable state, so they are prefer to aggregate to minimize the total surface energy [12]. While, it has been proved that the physicochemical properties of metal nanoparticles are size and shape dependent [13].

Recently, enormous interests have been drawn for the development of reduced graphene oxide based nanoparticle composites. Since abundant functional groups on the surfaces of GO can act as nucleation centers or anchoring sites for the landing of nanoparticles, limiting the nanoparticles growth, improving the stability and dispersion of nanoparticles on rGO nanosheets. At the same time, these nanoparticles can aid to enlarge the interplanar spacing of the rGO especially when they are in solid state. Therefore, prevent the aggregating of rGO into graphitic structure, and maintain the excellent properties of individual rGO

* Corresponding author at: Sonochemical Research Center, Department of Chemistry, Faculty of Science, Ferdowsi University of Mashhad, 91779 Mashhad, Iran.
E-mail addresses: entezari@um.ac.ir, moh_entezari@yahoo.com (M.H. Entezari).

https://doi.org/10.1016/j.ultsonch.2018.01.020
Received 31 July 2017; Received in revised form 16 January 2018; Accepted 26 January 2018

nanosheets [14–17]. However, the developed ways suffer from the employ of hazardous or toxic reducing agents such as $NaBH_4$ and formaldehyde to reduce both GO and Ag^+ ion, posing environmental and health risks, or the involvement of a surface modifier such as poly(N-vinyl-2-pyrrolidone) (PVP) [18].

Up to now, a variety of methods, such as electrochemical, chemical vapor deposition, ion exchange, hydrothermal, sol–gel, gamma irradiation and sonochemical methods have been applied to incorporate nanoparticles inside graphene sheets. Among the different approaches, sonochemistry has become an important method for the reduction of metal precursors and graphene oxide to rGO to get a homogeneous dispersion of exfoliated graphene sheets with metal nanoparticles [19–22]. The chemical effects of ultrasound irradiation is due to the acoustic cavitation phenomenon. When a liquid is irradiated with ultrasound, bubbles are created, growth and subsequent collapse, which leads to the release of the accumulated ultrasonic energy within a very short time. The extremely high local temperature (> 5000 K), pressure (> 20 MPa) and very high cooling rates ($> 10^{10}$ K s^{-1}) are suitable conditions for reducing GO and metal ions. Furthermore, the shear forces caused by acoustic cavitation are sufficient to overcome the van der Waals interaction between graphene sheets.

4-Nitrophenol (4-NP) is one of the most toxic and refractory pollutant in wastewater which derived from the industrial manufacturing processes of agrochemicals, pigments and pharmaceuticals. Instead, 4-aminophenol (4-AP) is very beneficial and important in many fields that include analgesic and antipyretic drugs, photographic developer, corrosion inhibitor, anticorrosion lubricant. Although there are many routes for removal of hazardous 4-NP but its catalytic reduction to 4-AP over appropriate catalyst (e.g. metal and metal oxide nanoparticle) has become a hot research topic [23–26].

Regarding the above description, the present research focuses on the use of ultrasonic irradiation to achieve the uniform loading of Ag nanoparticles on rGO nanosheets. Ag nanoparticles were chosen because among various kinds of noble metal such as Au, Pt, and Pd, they are low cost. In this work, a mild, inexpensiveness and environmental friendly reductant, diethylene glycol (DEG), was used as both reductive and dispersing agent. To the best of our knowledge, there has been no report on the sonochemical synthesis of Ag-rGO nanocomposites using DEG that does not involve chemical reducing and/or stabilizing agents. In comparison, the formation of rGO-Ag nanocomposite was accomplished by reflux precursor solution (classical method). Finally, catalytic activity of desired nanocomposites were investigated by reduction of 4-Nitrophenol in the presence of sodium borohydride ($NaBH_4$) as a model reaction.

2. Experimental

2.1. Materials

Graphite powder (purity 99%, mesh 325), potassium permanganate ($KMnO_4$), sulfuric acid (H_2SO_4, 98%), hydrochloric acid (HCl, 37%), ethanol (96%), silver nitrate ($AgNO_3$, 99%), 4-nitrophenol ($C_6H_5NO_3$, 99%) and sodium borohydride ($NaBH_4$, 98%) were provided from Merck. Diethylene glycol ($(HOCH_2CH_2)_2O$, 99%) and phosphoric acid (H_3PO_4, 85%) from Riedel, hydrogen peroxide (H_2O_2 30%) from Fluka company. All reagents were used directly without any further purification. Deionized water (DI) was used in the synthesis process.

2.2. Synthesis of graphene oxide (GO)

GO was obtained from the oxidation of graphite with the improved Hummers method [27]. Briefly, 1 g of graphite powder was mixed with a 9:1 mixture of concentrated H_2SO_4/H_3PO_4 (120/13.3 mL). Then 6 g $KMnO_4$ was added gradually under vigorous stirring, while temperature was kept below 20 °C to control the exothermic reaction. The reaction was oxidized for 12 h at 50 °C. Next, the mixture was cooled to room temperature and then 133 mL DI and 1 mL H_2O_2 was added to end the reaction. GO was collected by centrifuging the mixture and rinsed with 10% HCl and H_2O several times and then dried under vacuum.

2.3. Synthesis of rGO-Ag-C nanocomposite

First, 15 mg of graphene oxide was dispersed in 15 mL of DEG to form a stable GO colloid solution and 2.5 mL DI water was added to it (solution 1). Different amount of $AgNO_3$ (0.025–0.125 g) was dissolved in 7.5 mL DEG and then mixed with solution 1. After that, the mixture was stirred for 30 min to ensure the adsorption of Ag^+ ions on the surface of GO sheets. The reduction reactions were then performed at 150 °C for 3.5 h under constant stirring. At the end of the reactions, the mixture was cooled and products (rGO-Ag-C) were finally separated by centrifugation. Then the sample was washed with deionized water several times, and dried at 80 °C overnight. Following the above procedures, rGO nanosheets and Ag nanoparticles (Ag NPs) were prepared separately under the same conditions.

2.4. Synthesis of rGO-Ag-U nanocomposite

The solutions for the ultrasonic reduction were produced by the similar way with classical method. After magnetic stirring the mixture for 30 min, the resulting suspension was exposed to sonication using an ultrasonic horn (20 kHz, Branson Digital Sonifier-USA, W-450D) in a Rosset cell. Various amplitudes (50%, 60% and 70%) for 10 min were applied to deliver different acoustic power of 20.1 W, 24.5 W and 29.9 W, respectively. Ultrasonic waves applied in pulse mode with a 3-s pulse and 3-s relaxation cycle. Finally, the samples (rGO-Ag-U) were separated, washed with DI water and dried at 80 °C overnight. The ultrasonic process was conducted without any cooling. Therefore, a temperature of about 40 °C was reached after 10 min at the end of the reactions. The fabrication process for rGO-Ag-C and rGO-Ag-U nanocomposites are outlined in Fig. 1.

2.5. Analysis instruments

To investigate the optical properties of the samples, UV–Vis spectra were collected on a Unico 2800 spectrophotometer with 1 cm quartz cells. Fourier transform infrared (FT-IR) spectrum was done on a Thermo Nicolet 370 spectrometer in KBr medium in the region of 500–4000 cm^{-1}. The crystal structure of the as-prepared powders were determined by X-ray diffractometer (XRD, Explorer, JNR) equipped with Cu Kα radiation ($\lambda = 0.15406$ nm) over 2θ range of 5–90° at a scanning rate 0.05° s^{-1}. The morphology and structure of as-prepared particles were examined by transmission electron microscopy (TEM, Philips BioTwinCM120). Samples for TEM analysis were prepared by depositing a single drop of diluted sample dispersion in ethanol on carbon-coated grids. Energy dispersive X-ray spectroscopy (EDX) analysis coupled to the SEM instrument was carried out to study the elemental composition of the nanocomposites. The Raman spectra was recorded using a Teksan Takram P50C0R10 spectrometer with a 532 nm YAG laser as the excitation source. The specific surface area of the products were investigated by the Brunauer–Emmett–Teller (BET) method on the basis of nitrogen adsorption-desorption isotherms measured at 77 K using a BELSORP-mini analyzer.

2.6. Catalytic reduction of 4-NP

Catalytic efficiency of the resultant nanocomposites were evaluated by employing the reduction of 4-nitrophenol to 4-aminophenol in the presence of excess $NaBH_4$, which is a well-known model reaction. Briefly, 0.05 g $NaBH_4$ was added to 25 mL of 0.2 mM 4-NP aqueous solution with continuous stirring in a 50 mL beaker under ambient conditions. And then, special amount of the rGO-Ag-C and rGO-Ag-U powders (1–4 mg) were added to above mixture in different series of

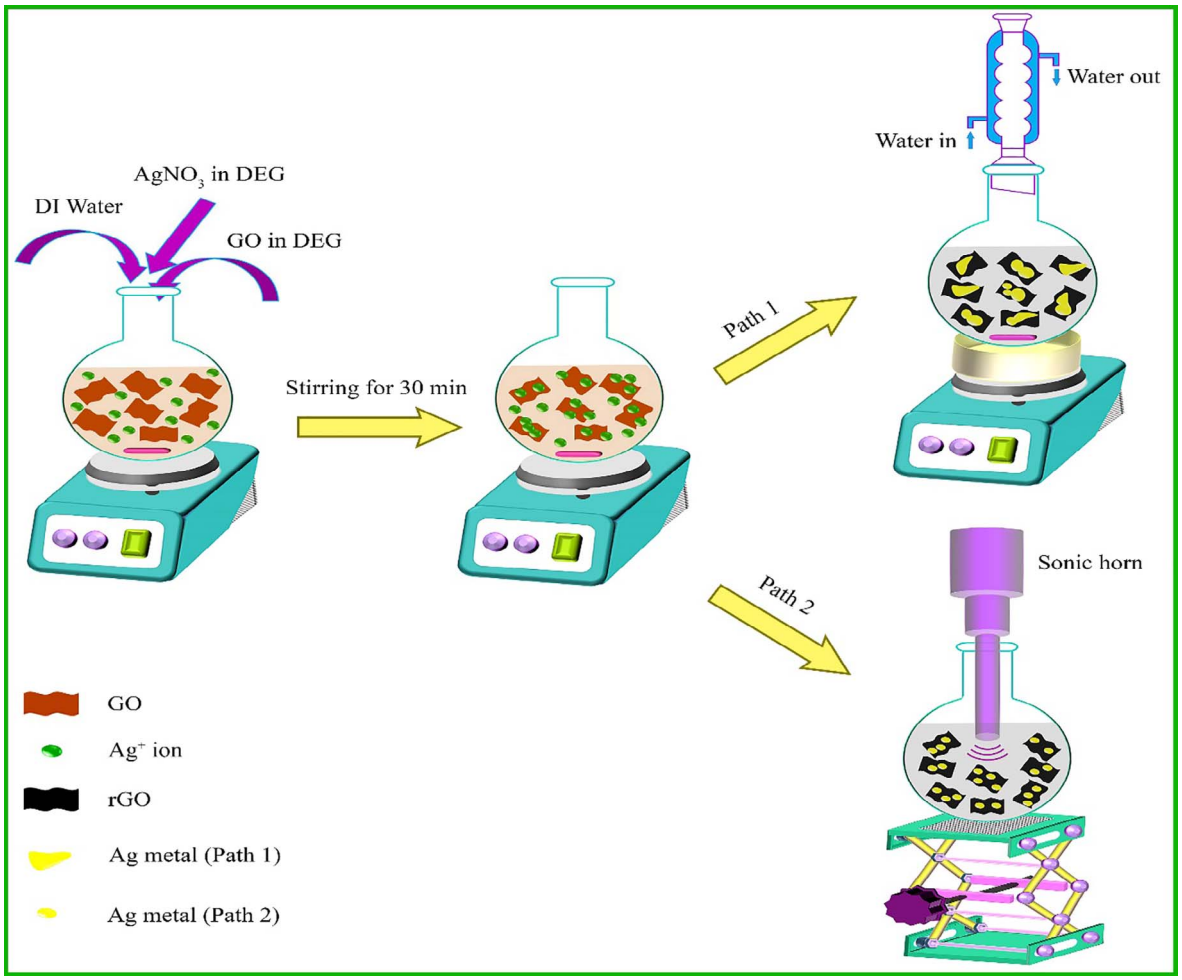

Fig. 1. Schematic representation of the preparation of rGO-Ag by classical (path 1) and ultrasound (path 2) methods.

experiments. A portion of the reaction mixture were collected at a regular time interval and the solids and liquid were separated rapidly by centrifugation for UV–Vis spectroscopy analysis. To study the stability and reusability of catalysts, once the reaction was completed, catalyst was isolated, then washed with water and dried at 80 °C for the next reduction reaction.

3. Results and discussion

To produce graphene-based nanocomposites, graphene oxide is usually chosen as a direct starting material, because it possesses lots of oxygen-contained functional groups which allows for appropriate synthesis of nanocomposites. GO nanosheets have large surface areas and both sides of nanosheets are available. Also, large-scale production of GO is possible by oxidation of natural graphite with strong oxidants [16].

Adding a small amount of water during the reduction process has several advantages. Primarily, it can aid to form homogeneous colloidal suspensions of GO. Secondly, it may buffer the formation rate of the metal particles, hence control the particle size at a specified range [28].

3.1. Optimization of rGO-Ag-C synthesis conditions

To obtain the optimum conditions for the synthesis of rGO-Ag-C, the amount of $AgNO_3$, temperature and reaction time were altered. The performance of the samples were evaluated by catalytic reduction of 4-NP in the presence of $NaBH_4$. The results are listed in Table 1.

As seen in Table 1, the catalytic performance of the samples increases with $AgNO_3$ amount from 0.025 to 0.05 g (samples C_1, C_2), but decreases in amount above 0.05 g (samples C_3, C_4 and C_5). The UV–Vis spectroscopy is a very useful technique to track the size evolution of silver nanoparticles based on localized surface plasmon resonance band exhibiting at different wavelength. As shown in Fig. 2a, Ag nanoparticles exhibit a weak absorption peak at 420 nm, a sharp extinction peak at 420, 424, 429 and 436 nm for the samples C_1, C_2, C_3, C_4 and C_5, respectively. It is well known that the absorption maxima of metallic nanoparticles shifted to longer wavelength with increase in nanoparticle size. The silver nanoparticles concentration which loaded on the rGO nanosheets raises with increasing the amount of $AgNO_3$. However, the Ag NPs size becomes larger at higher amount of $AgNO_3$ and causing loss of catalytic activity [29]. Therefore, the amount of 0.05 g $AgNO_3$ was selected for subsequent experiments.

Table 1
Synthesis conditions for the rGO-Ag-C, and their efficiency in the catalytic reduction of 4-NP.

Sample	$AgNO_3$ (g)	Temperature (°C)	Time (h)	k_{app} (min^{-1})
C_1	0.025	125	3.5	0.074
C_2	0.05	125	3.5	0.123
C_3	0.075	125	3.5	0.069
C_4	0.1	125	3.5	0.062
C_5	0.125	125	3.5	0.059
C_6	0.05	150	3.5	0.180
C_7	0.05	175	3.5	0.142
C_8	0.05	150	2	0.090
C_9	0.05	150	6	0.128

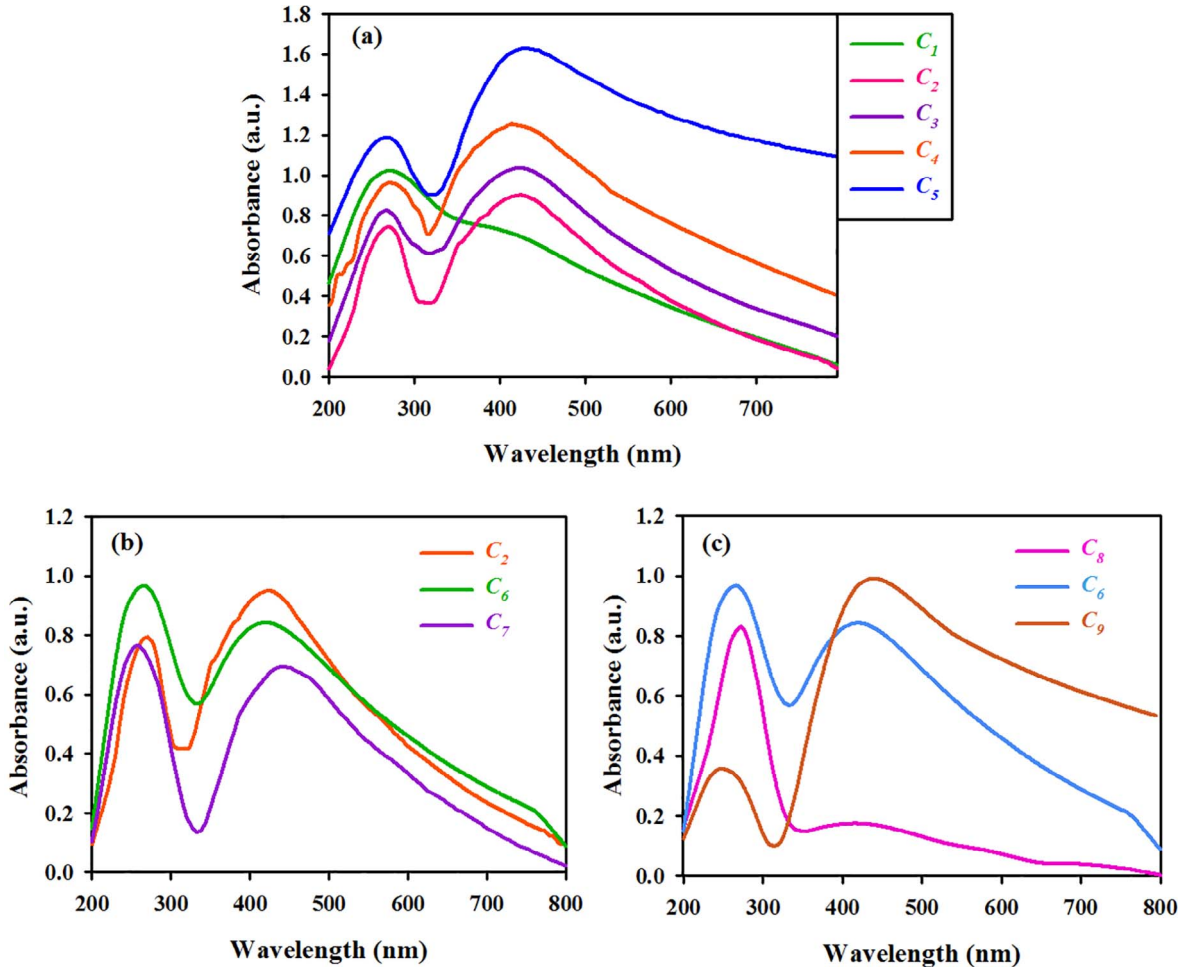

Fig. 2. UV–Vis spectra of the rGO-Ag-C nanocomposites synthesized under different conditions; (a) amount of $AgNO_3$, (b) temperature, and (c) time of reaction.

In the samples of C_2, C_6 and C_7 the effect of reaction temperature was studied on the synthesis of catalyst at 125, 150 and 175 °C, respectively. According to Table 1, the rate constant of reduction reaction of 4-NP was increased from 125 to 150 °C and reduced at 175 °C. The UV–Vis spectra (Fig. 2b) of the samples show that such trends could be attributed to the size of Ag NPs. Generally, the size of metal nanoparticles depends on the competition between nucleation and growth process. In the nucleation process, metal ions are reduced in the bulk solution and produced new particles. Whereas in the growth process, metal ion reduction occurs on the nuclei and/or small particles and so increasing the nanoparticle's size would be more significant. As the reaction temperature increases, the reaction rate (the rate of adsorption of Ag^+ ions on GO surface) increases and most silver ions to be consumed in the formation of nuclei; thereby stopping the growth process on the surface of the preformed nuclei and smaller particles are formed (maximum absorption occurred at 415 nm). Increasing the temperature beyond the optimal point (150 °C) aids the growth of the crystal around the nucleus and absorption peak red shifted to 450 nm [30,31]. In addition, GO is a thermally unstable material, hence quickly reduced to rGO at higher temperatures [21].

In order to assess the effect of reaction time on the synthesis of rGO-Ag-C, the reaction was conducted at 2, 3.5 and 6 h (samples C_8, C_6 and C_9, respectively) without changing any other parameters. The results show that the rate of 4-NP reduction increases as a function of reaction time. The UV–Vis spectra of the samples (Fig. 2c) show that increasing the reaction time from 2 to 3.5 h leads to increase the Ag NPs concentration on the surface of rGO nanosheets; hence improved the catalytic performance. However, at higher reaction time, the growth process were dominant, thus increased the size of Ag NPs.

3.2. Optimization of rGO-Ag-U synthesis conditions

In the ultrasonic irradiation process, the localized hotspots with a high temperature of 5000 K generated due to the rapid collapse of cavitation bubbles. Under this condition, water molecules homolysis into highly reactive $H^{\cdot}$ and $OH^{\cdot}$ radicals [21],

$$H_2O \rightarrow H^{\cdot} + OH^{\cdot} \quad (1)$$

$H^{\cdot}$ is known as one of the strongest reducing agnates. On the other hand, in the presence of DEG, the following reactions proceed [19],

$$H\text{-}(OCH_2CH_2)_2\text{-}OH + OH^{\cdot} \rightarrow H\text{-}(OCH_2C^{\cdot}H)_2\text{-}OH + H_2O \quad (2)$$

$$H\text{-}(OCH_2CH_2)_2\text{-}OH \rightarrow \textit{organic pyrolysis radicals} \quad (3)$$

In fact, DEG serves as $OH^{\cdot}$ radical scavengers to prevent oxidation of small silver nanoparticle to form silver oxide and a secondary radical ($H\text{-}(OCH_2C^{\cdot}H)_2\text{-}OH$) was formed (Eqs. (2)). The secondary radical exhibits strong reducing power [32]. In addition, the pyrolysis of the organic solute within the bubbles generated reducing radicals (Eqs. (3)) [19]. The $H^{\cdot}$, secondary and organic pyrolysis radicals that are produced can subsequently reduce the GO and Ag^+ ions.

$$GO + Ag^+ + \textit{reducing radicals} \rightarrow Ag(0) + rGO \quad (4)$$

In case of ultrasound, the effect of different parameters such as sonication time, ultrasonic amplitude, reaction temperature, and amount of $AgNO_3$ on the synthesis of nanocomposites and their catalytic activity have also been examined. The results are listed in Table 2.

Table 2
Synthesis conditions for the rGO-Ag-U, and their efficiency in the catalytic reduction of 4-NP.

Sample	Time (min)	Amplitude (%)	Temperature (°C)	$AgNO_3$ (g)	k_{app} (min^{-1})
U_1	3	70	25	0.05	0.250
U_2	5	70	25	0.05	0.290
U_3	10	70	25	0.05	0.371
U_4	20	70	25	0.05	0.310
U_5	30	70	25	0.05	0.289
U_6	10	60	25	0.05	0.308
U_7	10	50	25	0.05	0.227
U_8	10	70	40	0.05	0.192
U_9	10	70	55	0.05	0.150
U_{10}	10	70	$T_i = 25$, $T_f = 40^*$	0.05	0.740
U_{11}	10	70	$T_i = 25$, $T_f = 40^*$	0.01	0.472
U_{12}	10	70	$T_i = 25$, $T_f = 40^*$	0.025	1.180
U_{13}	10	70	$T_i = 25$, $T_f = 40^*$	0.1	0.670

* The ultrasonic process was conducted without any cooling. So the temperature increased at the end of the reaction.

First, to study the effect of sonication time on the synthesis of rGO-Ag-U, five samples containing 0.05 g $AgNO_3$ are irradiated at amplitude of 70% for 3, 5, 10, 20, and 30 min at 25 °C (samples U_1, U_2, U_3, U_4 and U_5, respectively). It is found that with increase of the sonication times from 3 to 10 min, the rate constant of 4-NP reduction enhanced, however, sonication for longer times has a negative effect on the reduction of 4-NP. The UV–Vis spectra of the samples U_1 and U_2 (Fig. 3a) show a weak absorption peak at 360 nm, related to the Ag NPs. However in the sample U_3 the absorption peak of Ag NPs was not visible, but the absorbance around 350–400 nm increased. The absence of Ag NPs' peak can be explained by the small size of Ag NPs [33]. Loss of catalytic activity of the samples U_4 and U_5 may be occurred due to aggregation of Ag NPs with prolonging of ultrasonic irradiation time and created a larger Ag NPs.

To obtain the optimum amplitude for the synthesis of rGO-Ag-U with high catalytic efficiency, samples were irradiated at 50%, 60% and 70% amplitudes for 10 min at 25 °C (samples U_7, U_6 and U_3, respectively). The results clearly show that the rate constant of 4-NP reduction was increased from 0.227 to 0.371 min^{-1} by applying an ultrasonic amplitude from 50% to 70%. It is well known that the size of Ag NPs depends upon the ultrasonic irradiation amplitude because the amounts of H ˙and organic pyrolysis radicals (reducing agents in the ultrasound process) are closely related with ultrasonic irradiation amplitude. At higher ultrasonic amplitudes, higher concentrations of reactive radical species are formed [34]. These species rapidly promote the reduction of Ag^+ ions. Since the size of the Ag NPs obtained at high ultrasound amplitude was smaller than that of the Ag NPs obtained at low ultrasound amplitude [35]. In addition, the reactive radical species also play an important role in the reduction of GO into graphene. With increasing the concentration of radicals, the reduction degree of rGO increases too. On the other hand, since the amount of radicals generated at low amplitude is less, the reduction of Ag^+ ion is slow and the coagulation of Ag NPs occurs. As shown in Fig. 3b, the absorbance related to Ag NPs increased with increasing an ultrasonic amplitude from 50 to 70%. In addition, the absorption peak of rGO red shifted from 235 to 265 nm with increasing amplitude, which indicate that the reduction degree of

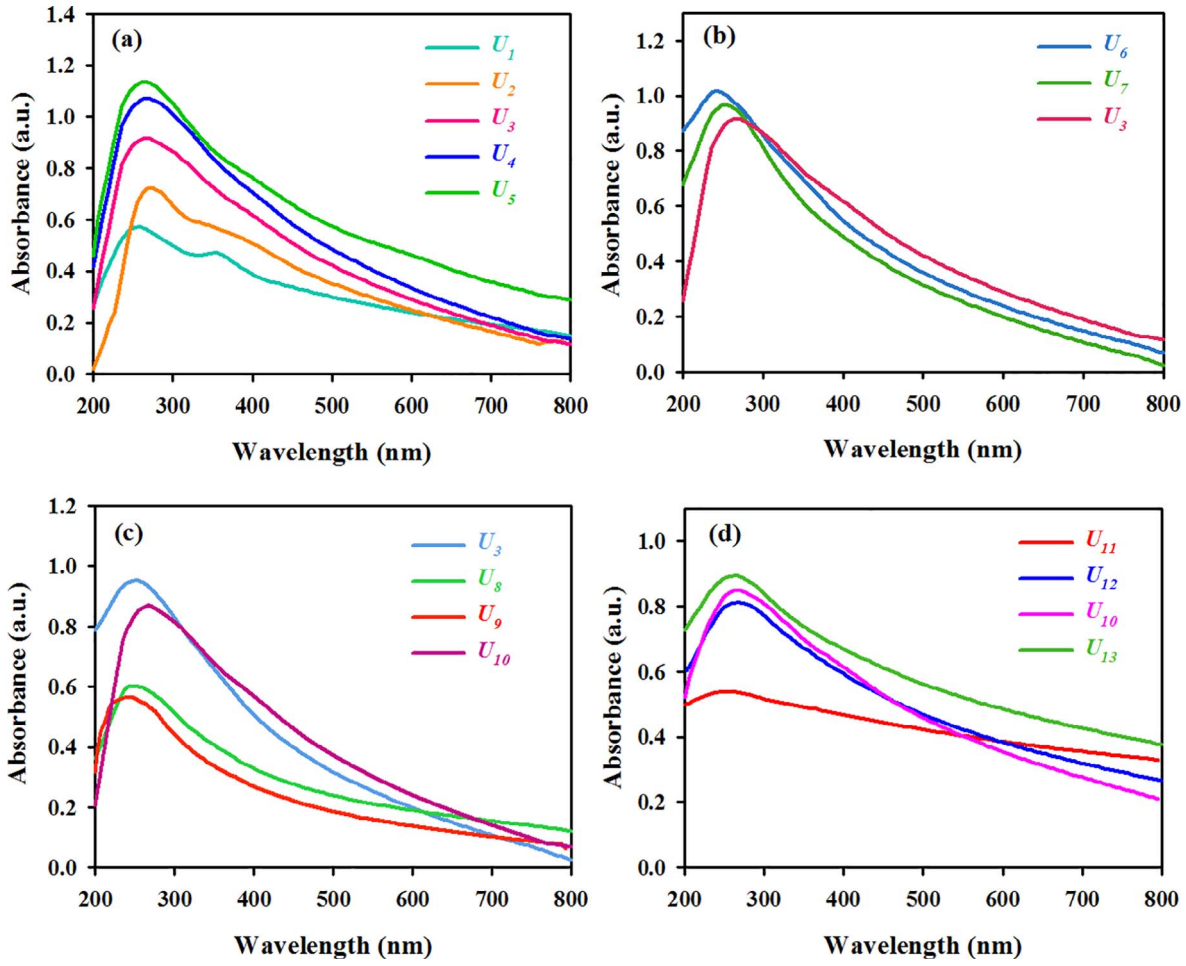

Fig. 3. UV–Vis spectra of the rGO-Ag-U nanocomposites synthesized under different conditions; (a) ultrasonic irradiation times, (b) ultrasonic amplitude, (c) temperature, and (d) amount of $AgNO_3$.

rGO increases.

In order to understand the effect of temperature, the rGO-Ag-U were synthesized at 25, 40 and 55 °C and the temperature was controlled through the circulating water (samples U_3, U_8 and U_9). Another sample was also prepared by applying the ultrasound without any temperature control and hence a temperature of about 40 °C was reached after 10 min sonication at 70% amplitude (sample U_{10}). Table 2 shows that the catalytic performance decreased from the sample U_3 to U_8 and U_9, but increased in the sample U_{10} from 0.371 to 0.74 min^{-1}. This behavior could be explained by the effect of temperature on the cavitation process. When the temperature increased, the water and DEG molecules are easily vaporized and filled inside the cavitation bubbles. In result, the collapse of bubbles is not effective for generation of reducing radicals [31]. The UV–Vis analysis (Fig. 3c) also indicated the absorbance of Ag NPs decreases with increasing the temperature.

Another parameter that can be optimized is the amount of $AgNO_3$. Samples (U_{10}, U_{11}, U_{12} and U_{13}) containing 0.01 to 0.1 g of $AgNO_3$ are prepared and irradiated for 10 min. From Table 2, the rate constant of 4-NP reduction raises from 0.74 to 1.18 min^{-1} with increase of the amount of $AgNO_3$ from 0.01 to 0.025 g. However, the rate of 4-NP reduction was found to decrease at higher amount of $AgNO_3$. Fig. 3d indicated that the absorbance of silver nanoparticles increased with increasing the amount of $AgNO_3$ from 0.01 to 0.025 g. However, in the amount of $AgNO_3$ above 0.025 g, a significant change was not observed in the UV–Vis spectra of the samples and loss of catalytic activity may be attributed to increasing the size of Ag NPs.

Based on experimental data, the optimum conditions for the synthesis of rGO-Ag-C were as follows: 0.05 g of $AgNO_3$, 150 °C, and 3.5 h reaction time. It is remarkable that rGO-Ag-U was synthesized in very easier conditions: 0.025 g of $AgNO_3$, 10 min sonication time, and 70% amplitude.

3.3. Characterization of optimized rGO-Ag-U and rGO-Ag-C

The crystalline nature of the products was determined using XRD analysis. Fig. 4a shows the XRD patterns of the pristine GO and rGO. The pristine GO has a sharp peak at $2\theta = 10.6^{\circ}$ which corresponds to (0 0 2) plane. After the reduction of GO by DEG, the peak at 10.6° disappears and a new peak at $2\theta = 20–30^{\circ}$ appears. This weak and broad diffraction peak is originated from the (0 0 2) plane of rGO nanosheets [18]. For the rGO-Ag-C and rGO-Ag-U (Fig. 4b), four peaks located at 38.05, 44.23, 64.50, and 77.56° are assigned to (1 1 1), (2 0 0), (2 2 0), and (3 1 1) plans of fcc Ag NPs, respectively. As well as, the peaks at 32.2 and 54.6° in the rGO-Ag-U is related to (1 0 1) and (1 4 2) faces of Ag NPs [36,37]. The characteristic diffraction peak of rGO is absent in the XRD patterns of rGO-Ag-C, which may be attributed to relatively low diffraction intensity of graphene sheets [14].

Fig. 5 displays the TEM images of the as-synthesized samples. As depicted in Fig. 5a, the rGO nanosheets are ultrathin and transparent with some wrinkles and folded regions. For the rGO-Ag-C and rGO-Ag-U, it can be seen that the surface of rGO is decorated with Ag NPs with different particle size distributions. In case of rGO-Ag-C (Fig. 5b), large Ag NPs have been formed on the surface of rGO nanosheets. On the other, in the sample of rGO-Ag-U (Fig. 5c), Ag NPs with small size uniformly decorated on rGO nanosheet and no Ag nanoparticles with obvious aggregation are identified. The particle size distribution (Fig. 5d) showed that Ag NPs with an average diameter of 18 nm anchored on rGO by ultrasound method. In most cases, the surface passivation reagents such as surfactants and polymers were used to prevent the aggregation of metal nanoparticles owing to their high surface energy. Due to the absence of stabilizing agents during the synthesis process, aggregation of nanoparticles occurs in the classical method and leads to formation of larger Ag NPs. However, in the ultrasound method, the shock waves and micro jets induced by the bubble collapse during the cavitation process were dominated to the surface energy of Ag NPs and responsible to uniform and fine distribution of Ag NPs in the rGO-Ag-U.

Fig. 6 shows the typical EDX spectrum of rGO-Ag-C and rGO-Ag-U. From Fig. 6a and b, it was obvious that the elements Ag, C, and O were present in the nanocomposites. Peaks associated with C and O were resulted from rGO and Ag resulted from Ag NPs. The results confirmed the formation of Ag nanoparticles on rGO nanosheets. Furthermore, from this analysis, the weight percentage of Ag was determined to be 9.12% in the rGO-Ag-U and 33.89% in the rGO-Ag-C.

Fig. 7a indicates FT-IR spectra of GO, rGO and the as-prepared rGO-Ag via ultrasound and classical methods. The FT-IR spectra of GO containing a broad peak at 3300–3400 cm^{-1} which is attributed to the O—H stretching vibrations due to the adsorbed water on the surface of GO. Also, the characteristic peaks at 1731.64 cm^{-1}, 1619.67 cm^{-1}, 1222.97 cm^{-1} and 1043.37 cm^{-1} are related to C═O stretching vibrations, unoxidized sp^2-hybridized C═C and O—H bending, C—O—C stretching vibration (epoxy group), and C—O functional group, respectively [15,34]. After reduction (samples rGO, rGO-Ag-U and rGO-Ag-C), some of the above oxygen related functional groups disappeared or reduce in intensity. The results implies that GO has been successfully reduced by ultrasound and classical methods.

Raman spectroscopy is a powerful nondestructive tool to identify the ordered and disordered crystal structures of carbonaceous materials. As seen in Fig. 7b, the Raman spectra of GO shows two peaks at 1345 (D band) and 1587 cm^{-1} (G band). The D band arises from the vibrations of sp^3 carbon atoms of defects and disorder, and the G band is related to sp^2 bonded carbon atoms in a hexagonal lattice [6,19]. The Raman spectrum of the nanocomposits shows the G band at 1592 cm^{-1} and the D band at 1355 and 1361 cm^{-1} for rGO-Ag-C and rGO-Ag-U, respectively. The D and G bands intensity ratios (I_D/I_G) is a measure of the relative concentration of local defects or disorders compared with sp^2 hybridized graphene domains, hence the I_D/I_G ratio should decrease due to the restoration of sp^2 domains [26,38]. The I_D/I_G ratios are 1.03, 0.91 and 0.87 for GO, rGO-Ag-C and rGO-Ag-U, respectively. The decreased I_D/I_G ratios of nanocomposites in comparison with GO, indicated the reduction of GO during the classical and ultrasound reduction procedure.

To further confirm the reduction of GO and formation of Ag NPs, UV–Vis analysis was carried out as shown in Fig. 8a. GO possesses a sharp absorption peak at 225 nm due to the π-π^* transition of the C═C aromatic rings and the shoulder peak around 300 nm which is related to n-π^* transition of the C═O bonds. After reduction of GO to rGO, the peak at 225 nm in GO was red shifted to 270 nm which supports the restoration of sp^2 carbon atoms. Silver nanoparticles exhibited a characteristic absorption peak at 400 nm owing to their surface plasmon resonance. The spectrum of rGO-Ag-C, in addition of absorption peak of rGO, shows a peak at 415 nm due to the presence of Ag NPs on rGO matrix. In the spectrum of rGO-Ag-U, the absorption peak of Ag NPs was not visible, but the absorbance around 400 nm increased. The absence of Ag NPs peak can be explained by the small size of Ag NPs that have been obtained with ultrasound method [33].

The specific surface areas of the samples were calculated by BET technique. Based on N_2 adsorption-desorption isotherms (Fig. 8b) the BET surface area is determined 9.98, 11.09 and 24.59 $m^2 g^{-1}$ for GO, rGO-Ag-C and rGO-Ag-U, respectively. It is seen that the surface area of rGO-Ag-U was larger than rGO-Ag-C, which can be attributed to the tiny Ag NPs loaded on rGO by sonochemical method [39]. Moreover, the total pore volume of the GO, rGO-Ag-C and rGO-Ag-U were obtained 0.0284, 0.0545 and 0.1098 $cm^3 g^{-1}$, respectively, from the Barrett–Joyner–Halenda (BJH) plot (the inset in Fig. 8b).

3.4. Catalytic activity of rGO-Ag-C and rGO-Ag-U

The catalytic activity of the as-prepared rGO-Ag-C and rGO-Ag-U under optimized conditions were evaluated by reduction of 4-NP in the presence of excess $NaBH_4$. The selective reduction of 4-NP to 4-AP at room temperature is chosen widely as a model reaction to investigate

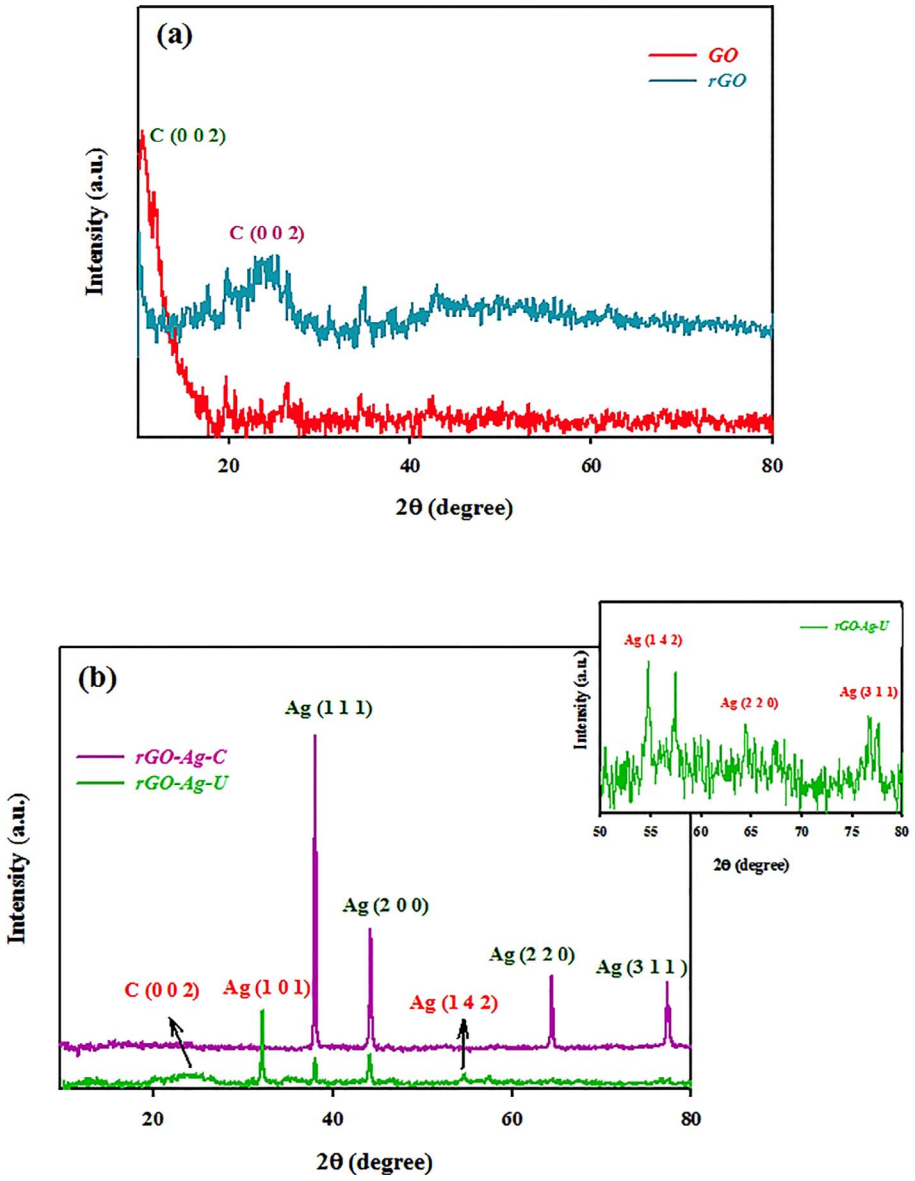

Fig. 4. XRD patterns of (a) principle GO and rGO nanosheets, (b) the as-synthesized rGO-Ag-C and rGO-Ag-U nanocomposites under optimum conditions.

the catalytic performance of metal nanoparticles.

It is noteworthy that the reduction of 4-NP in the presence of $NaBH_4$ is a thermodynamically feasible process ($\Delta E^\circ = E^\circ_{(4\text{-NP/4-AP})} - E^\circ_{(H3BO3/BH4)} = (-0.76) - (-1.33) = 0.67$ V), but it is kinetically restricted without catalysts due to the large kinetic barrier [40]. Normally, under neutral or acidic conditions, an aqueous solution of 4-NP shows a strong absorption peak at 317 nm and light yellow color (Fig. 9). It has been observed that upon the addition of $NaBH_4$, the solution color changed to intense yellow and the maximum peak at 317 nm red shifted to 400 nm due to the formation of 4-nitrophenolate ions in alkaline conditions.

In order to reduce 4-NP to 4-AP, 2 mg from each nanocomposites were added to the mixed solution of 4-NP and $NaBH_4$ at room conditions and the progress of the reduction reaction monitored by UV–Vis spectroscopy at regular intervals of time. As shown in Fig. 10, by addition of rGO-Ag-C and rGO-Ag-U in separate experiments, the intensity of the absorption peak at 400 nm gradually decreased as the reaction time increased, while a new peak appeared at 300 nm which corresponded to the formation of 4-AP. After 4 and 25 min (for rGO-Ag-U and rGO-Ag-C, respectively), the peak at 400 nm completely disappeared and yellow color of the solution was transferred to colorless. It was obvious that the as-prepared rGO-Ag via ultrasound method exhibited a better catalytic ability (about 6 times) for the reduction of 4-NP toward the as-prepared rGO-Ag via classical method. This could be ascribed to difference between the size of Ag NPs on the surface of rGO nanosheets which obtained by two methods. The small particles have more catalytic activity due to larger surface-to-volume ratio. In addition, larger specific surface area of the rGO-Ag-U cased more number of 4-NP molecules adsorb on the surface of catalyst for the next reduction reaction and therefore the catalytic activity increases. The presence of only two isosbestic points at 280 and 314 nm in the UV–Vis spectrum (Fig. 10), confirmed that 4-NP exclusively converted to 4-AP without any other by-product [41].

It is well known that the catalyst dosage is effective factor on the reduction of 4-NP to 4-AP. Hence, to evaluate the effect of the amount of catalyst, the reduction reaction was carried out under the same reaction condition while the amount of catalyst (both rGO-Ag-C and rGO-Ag-U) was varied from 1 to 4 mg. The catalytic reduction efficiency was determined by decreasing the absorption percentage at 400 nm in the first 2 min of reaction (Fig. 11). As shown in Fig. 11, with increasing the amount of catalyst from 1 to 2 mg, the conversion rate of 4-NP to 4-AP also increases duo to increase of surface active sites. When the amount

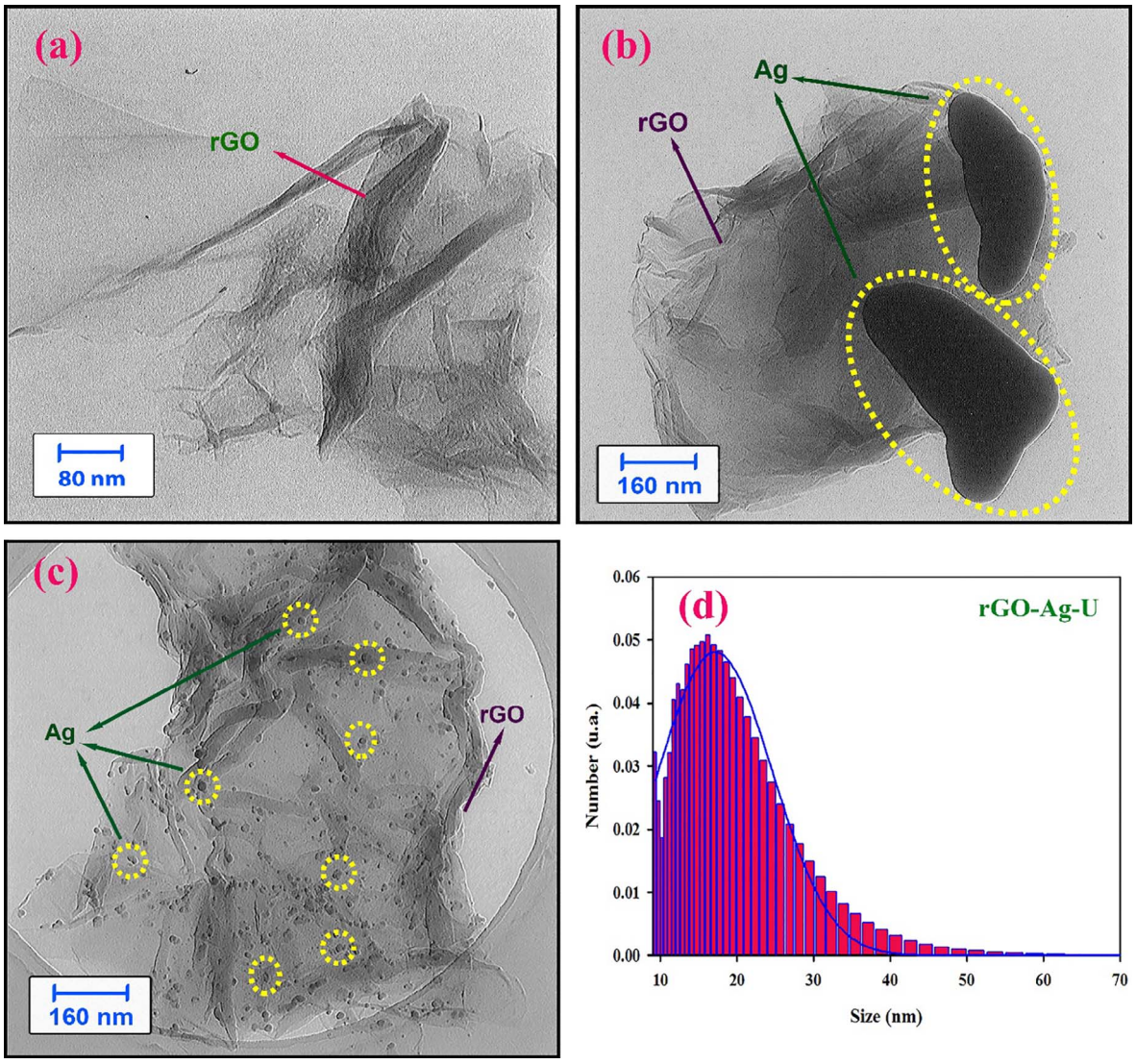

Fig. 5. TEM images of (a) rGO nanosheets, (b) rGO-Ag-C, and (c) rGO-Ag-U nanocomposites. (d) Particle size distribution of rGO-Ag-U.

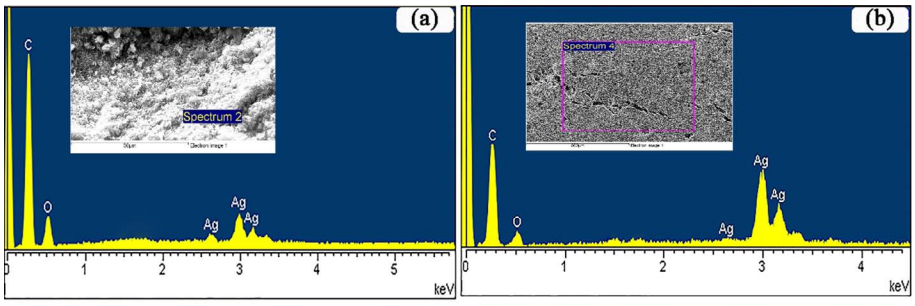

Element	C	O	Ag
Weight%	59.61	31.27	9.12
Atomic%	70.88	27.91	1.21

Element	C	O	Ag
Weight%	45.06	21.05	33.89
Atomic%	69.72	24.45	5.84

Fig. 6. EDX spectrum and chemical composition of the (a) rGO-Ag-U, and (b) rGO-Ag-C nanocomposites.

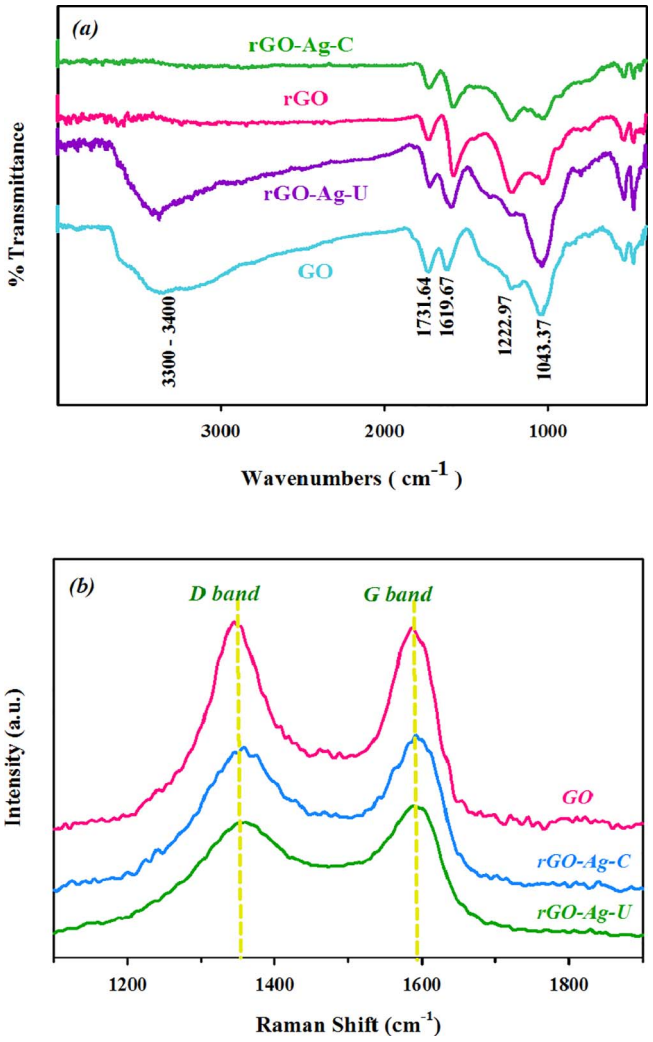

Fig. 7. (a) FT-IR spectra of the GO, rGO, rGO-Ag-U and rGO-Ag-C. (b) Raman spectra of the GO, rGO-Ag-C and rGO-Ag-U.

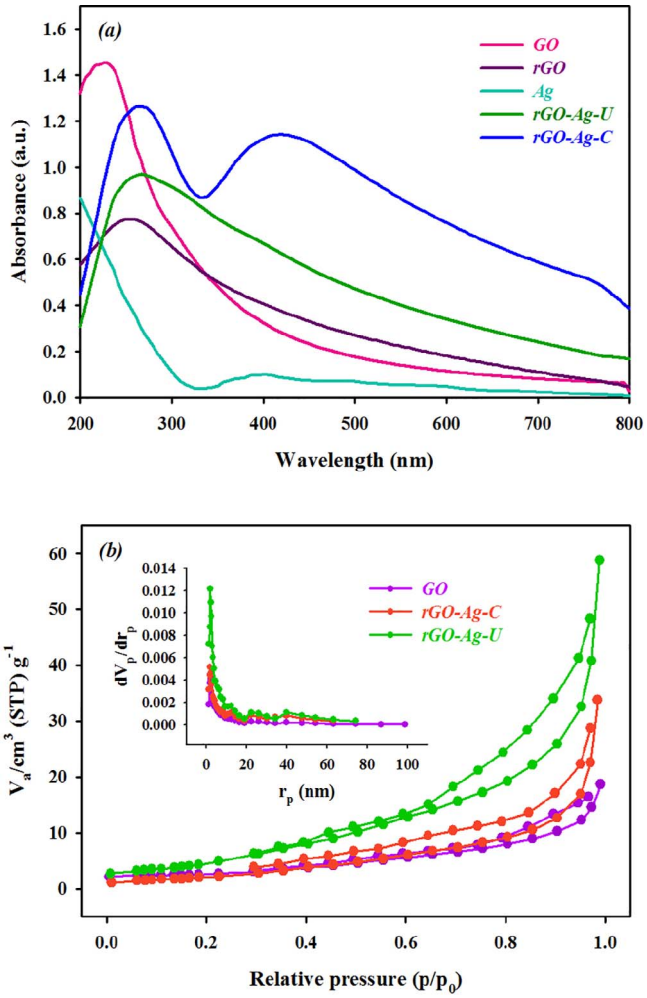

Fig. 8. (a) UV–Vis absorption spectra of the GO, rGO, rGO-Ag-U, and rGO-Ag-C. (b) Nitrogen adsorption-desorption isotherms of the GO, rGO-Ag-C, and rGO-Ag-U, the inset shows the Barrett-Joyner-Halenda (BJH) pore size distribution plot of samples.

of catalyst further increased to 4 mg, the conversion rate partially changed especially in case of rGO-Ag-U nanocomposites. In other words, in the amount of catalyst above 2 mg, mass of catalyst shows a decreased contribution to the catalytic activity [41]. Thus, the optimal catalyst dosage was chosen 2 mg.

3.4.1. Kinetics of reduction

As regards in the reduction process the initial concentration of $NaBH_4$ was very high, it can be considered constant throughout the reaction. Thus, the reaction was pseudo first-order and only dependent on the concentration of 4-NP [42]. Fig. 12 shows a linear correlation between ln (C_t/C_0), where C_0 is the initial concentration of 4-NP and C_t is the concentration of 4-NP at time t, and the reaction time at room temperature, confirms that the reduction follows a pseudo-first-order kinetics model:

$$ln(C_t/C_0) = -k_a ppt \quad (5)$$

Hence, the apparent rate constant (k_{app}) was calculated from the slope of a linear ln (C_t/C_0) verses t plot. From Fig. 12, the k_{app} was obtained to be 1.18 min^{-1} for rGO-Ag-U which was around 6.5 times higher than that obtained for rGO-Ag-C (0.18 min^{-1}). It was hypothesized that the smaller size of the Ag NPs contributed to the higher catalytic activity of rGO-Ag-U than the rGO-Ag-C [43].

For comparison, 4-NP reduction reactions by the individual components of the composite (GO, rGO, and Ag NP) were also performed under the same conditions. In all cases, it was observed that the intensity of the absorption peak at 400 nm decreased with different rates and a new peak appeared at 300 nm. Thus, the reduction of 4-NP can be occurred. As shown in Fig. 12, the catalytic efficiency of the rGO-Ag nanocomposites synthesized by ultrasound and classical methods were more than that of the other component materials.

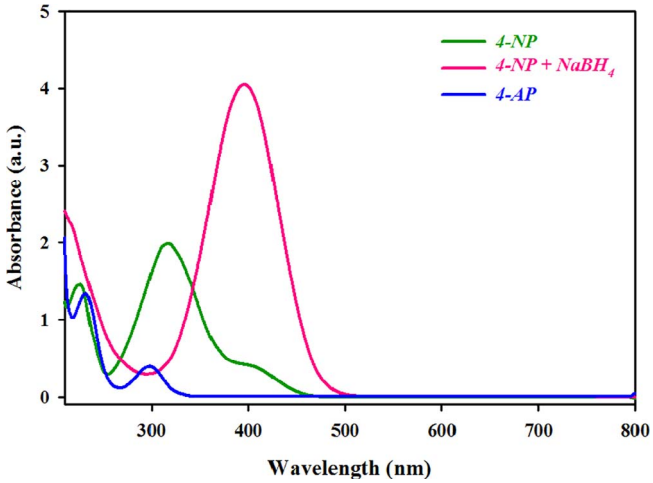

Fig. 9. UV–Vis spectra of 4-NP, 4-NP + $NaBH_4$, and 4-AP.

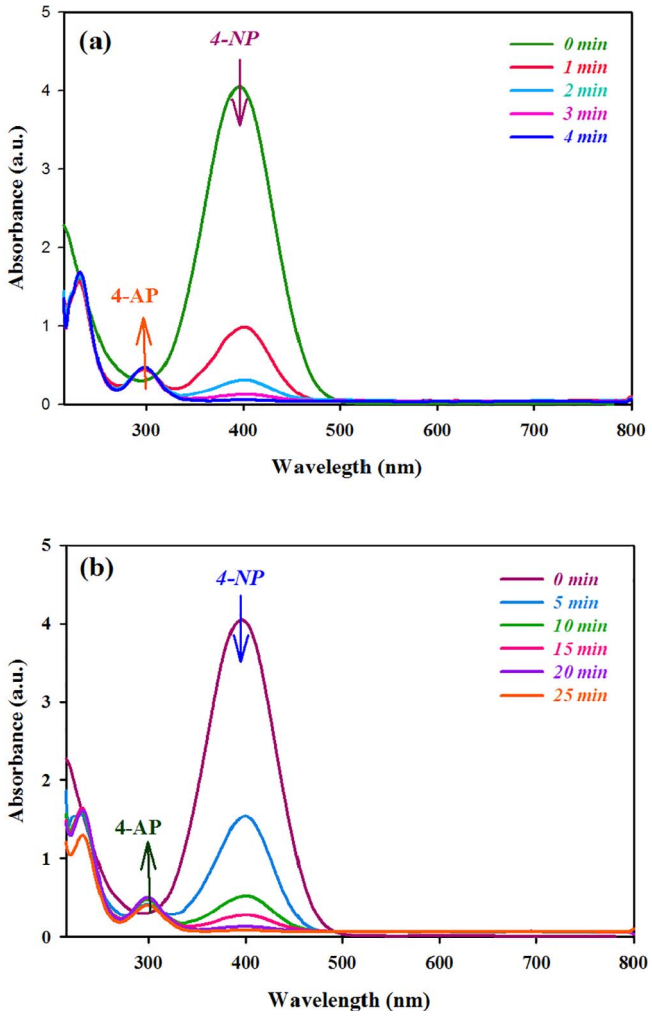

Fig. 10. UV–Vis absorption spectra of the reduction of 4-NP to 4-Ap by $NaBH_4$ in the presence of (a) rGO-Ag-U, and (b) rGO-Ag-C nanocomposites. (Reaction conditions: [4-NP] = 0.2 mM, $NaBH_4$ = 0.05 g, catalyst = 2 mg, and temperature = 25 °C).

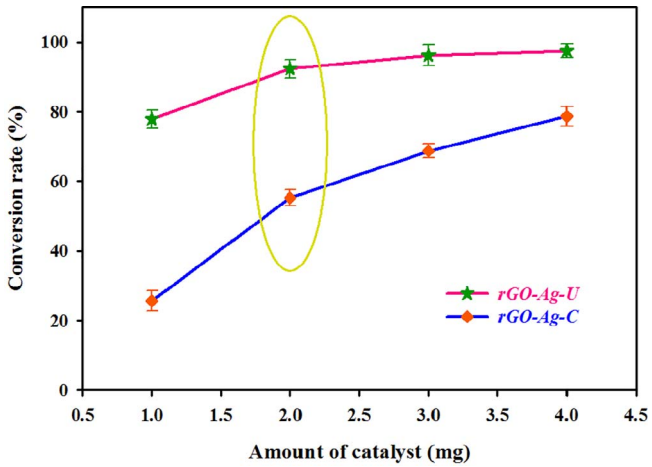

Fig. 11. Plots of conversion rate of 4-NP versus amount of catalyst in the first 2 min of reaction.

For comparison the catalytic activity of current catalysts with the ones reported in the literature, k_{app} is not appropriate, because it is related to the mass of the catalyst. The turnover number (TON) and the turnover frequency (TOF) of the catalyst are two important indicators that are usually used for comparing catalyst efficiency. In

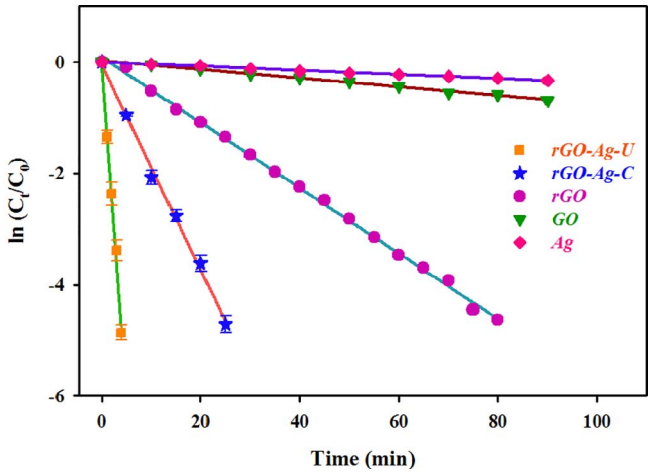

Fig. 12. Plots of ln (C_t/C_0) versus the reduction time of 4-NP to 4-AP catalyzed by rGO-Ag-U, rGO-Ag-C, rGO, GO, and Ag NPs. (Reaction conditions: [4-NP] = 0.2 mM, $NaBH_4$ = 0.05 g, catalyst = 2 mg, and temperature = 25 °C).

Table 3
Comparison of E_a and TOF of different catalytic systems for the reduction of 4-NP at 25 °C.

Nanocatalyst	E_a (kJ mol^{-1})	TOF (molecule g^{-1} s^{-1})	Reference
rGO-Ag-C	31.75	1.00×10^{18}	This work
rGO-Ag-U	25.57	6.25×10^{18}	This work
Ag-CA	–	9.3×10^{16}	[45]
Au-CA	–	1.7×10^{16}	[45]
Ag monolith	42.58	7.5×10^{17}	[44]
Pd-Ni/NrGO	29.1	–	[41]
$Cu_{2-x}Se$/rGO/PVP	49.05	–	[38]
Ag-PRGO	–	5.5×10^{18}	[12]
Au-PRGO	–	1.7×10^{18}	[12]

heterogeneous catalysis, the TON is the number of substrate molecules that 1 g of catalyst can convert into products. The TOF can be obtained by dividing TON on time [23,43]. The TOF values of the 4-NP reduction by rGO-Ag-U and rGO-Ag-C were estimated to be 6.25×10^{18} and 1.00×10^{18} molecules g^{-1} s^{-1} at room temperature, respectively. As reflected in Table 3, the current rGO-Ag-C and rGO-Ag-U nanocomposites show relatively higher catalytic activity for conversion of 4-NP to 4-AP.

Furthermore, activation energy (E_a) is an important kinetic parameter that exhibits the temperature dependency of rate constants in catalytic processes. The catalytic reduction of 4-NP by rGO-Ag-U and rGO-Ag-C were studied at various temperatures ranging from 15 to 55 °C and the corresponding k_{app} were investigated (Fig. 13). It was found that the k_{app} increased with increasing temperature. As shown in Fig. 13, the linear relationship between ln (C_t/C_0) and the reaction time t exhibits a classical Arrhenius-type dependence on temperatures, and the Arrhenius equation is as follows:

$$k = Ae^{(-Ea/RT)}, ln(k) = ln(A) - (E_a/RT)$$

Where k is the rate constant, A is the pre-exponential factor, R is the universal gas constant, T is the reaction temperature (in Kelvin) and E_a is the activation energy for the reaction. The E_a values for each nanocomposites were obtained from the slope of ln (k) versus 1/T plot (the inset in Fig. 13). The E_a for the catalytic reduction of 4-NP by rGO-Ag-U and rGO-Ag-C were calculated to be 25.57 and 31.75 kJ mol^{-1}, respectively. Usually, for the surface catalyzed reactions the value of E_a lies within 10–40 kJ mol^{-1} [41]. Therefore, the obtained values of E_a in this work indicated that the resulting catalysts can decreased the activation energy for the reduction of 4-NP to 4-AP by greatly lower the energy barrier compared to the other catalyst that reported in the literature (Table 3).

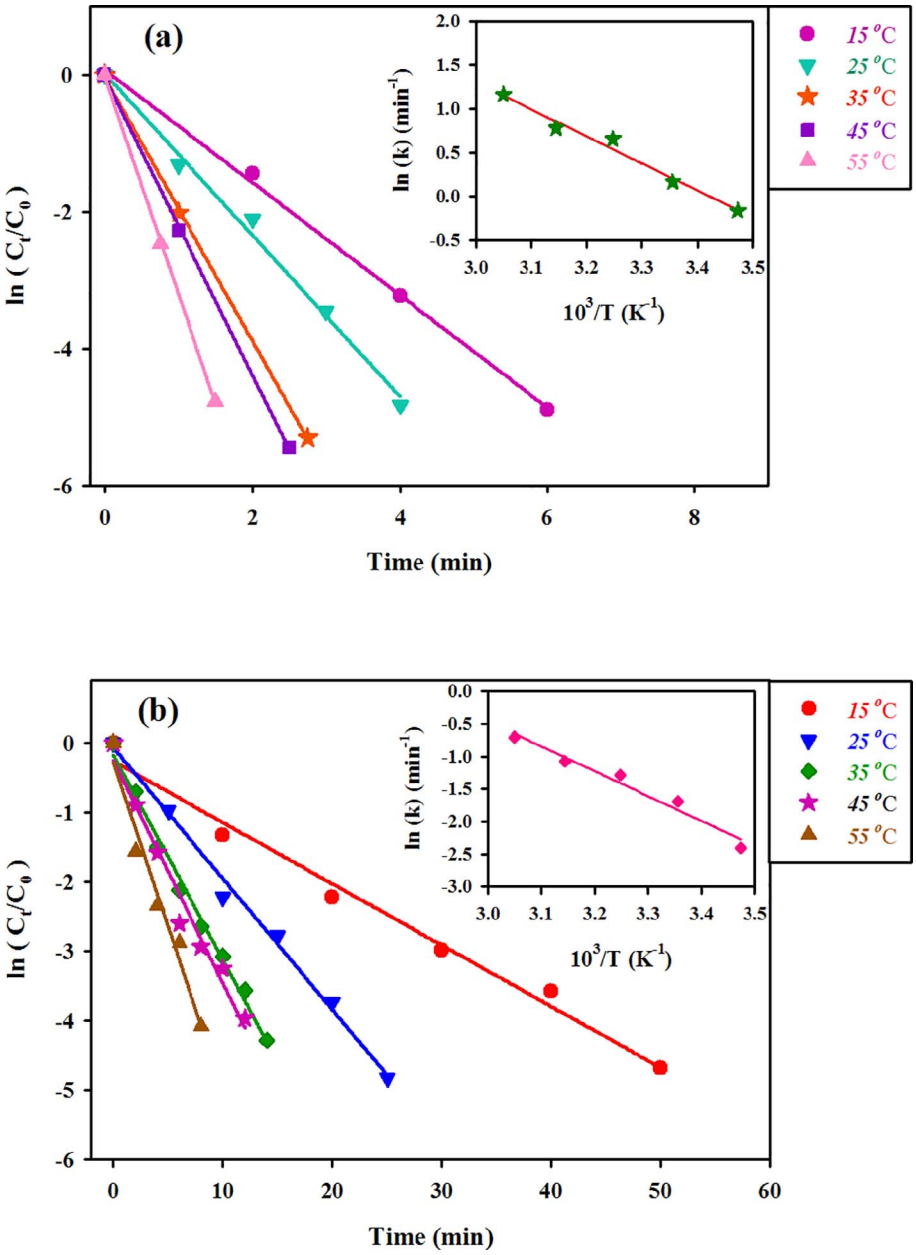

Fig. 13. Plots of ln (C_t/C_0) versus the reduction time of 4-NP to 4-AP at different temperature by (a) rGO-Ag-U, and (b) rGO-Ag-C nanocomposites. The inset shows the corresponding Arrhenius plot. (Reaction conditions: [4-NP] = 0.2 mM, $NaBH_4$ = 0.05 g, and catalyst = 2 mg).

Specifically, all of these results indicated that the rGO-Ag nanocomposite where obtained by the simple and fast ultrasound method exhibited a better catalytic performance for 4-NP reduction than the rGO-Ag-C.

3.4.2. Proposed mechanism

The experimental data confirmed that the as-prepared rGO-Ag nanocomposites by ultrasound and classical methods in the optimized conditions demonstrated the best performance for the reduction of 4-NP to 4-AP. Therefore, it is essential to explain the mechanism of reduction reaction. Fig. 14 shows the proposed mechanism of the rGO-Ag catalyst for the reduction of 4-NP. Generally it is accepted that the reduction of 4-NP by BH_4^- depends on two key factors: 1) the effective adsorption of reactants (4-NP and BH_4^-) on the surface of catalyst, 2) rapid hydrogen transfer from BH_4^- to 4-NP via the surface of catalyst [40].

In catalytic processes, the ability of catalyst for the adsorption is highly dependent on their surface area. Deposition of Ag NPs on the surface of rGO nanosheets, not only enhanced the dispersion and it also prevented the aggregation of Ag NPs especially for the rGO-Ag-U sample. Large surface area dramatically increased the adsorption abilities toward 4-NP by π-π stacking interactions. Such adsorption increased the local concentration of 4-NP near to the Ag NPs on the rGO nanosheets. On the other hand, BH_4^- ions as an electron donor adsorb on the surface of the Ag NPs. The electrons by cleavage of the B-H bond were transferred to Ag NPs, and hydrogen is released due to reduction of water to H_2 (step 1). In the presence of Ag NPs, the H—H bond in H_2 cleaves, and each active hydrogen attaches to the Ag NPs surface (step 2) [39,40]. It is reported that the active hydrogen is the exact species for the hydrogenation of 4-NP. The active hydrogen atoms react with 4-nitrophenolate ions, and ultimately in three step (step 3–5) reduce them into 4-AP. Eventually, the 4-AP molecules desorbed from the surface of catalyst (step 6) and dissolved in the solution, provide free surface of nanocomposites for the next catalytic cycle. The released bubbles during the reduction processes confirmed the presence of active

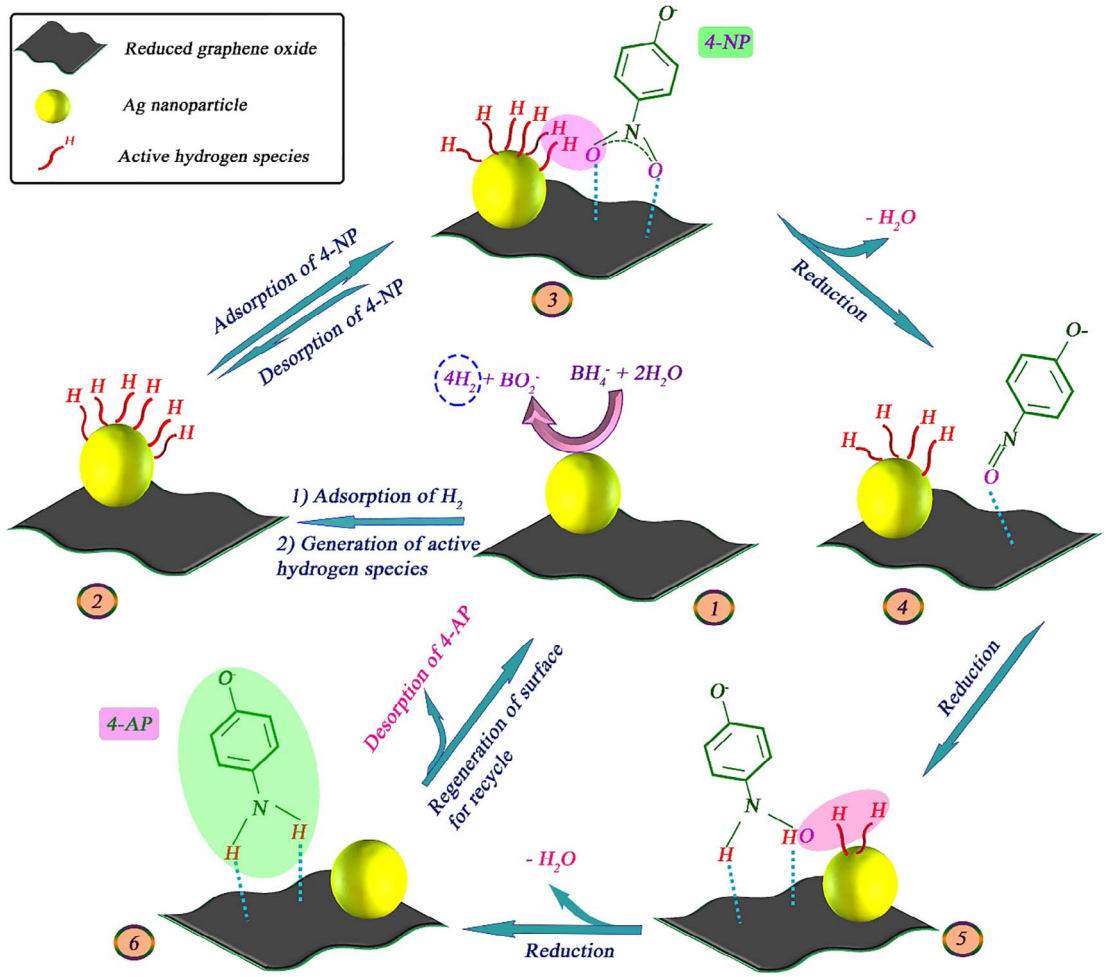

Fig. 14. Schematic representation of the proposed mechanism for the reduction of 4-NP to 4-AP over rGO-Ag nanocomposite in the presence of $NaBH_4$.

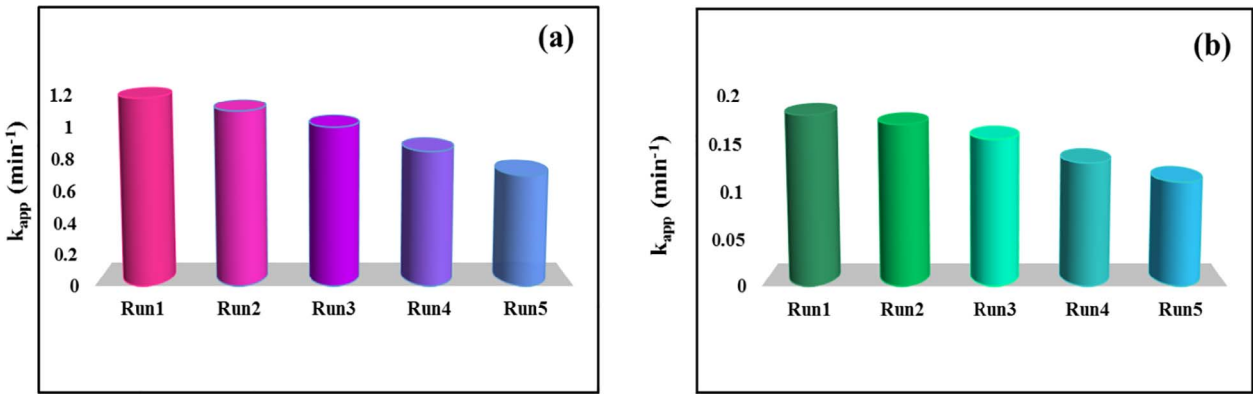

Fig. 15. Reusability of (a) rGO-Ag-U, and (b) rGO-Ag-C as the catalyst for the reduction of 4-NP to 4-AP in five cycles.

hydrogen, since the unreacted hydrogen species can combine with each other and generate H_2 gas [41].

3.4.3. Reusability of rGO-Ag-C and rGO-Ag-U

It is well known that the reusability of catalyst is a critical subject to practical applications of a catalyst. For this purpose, the as-prepared nanocomposites were applied to five cycle under the same reaction conditions. After each cycle the nanocomposite was isolated from the reaction mixtures by centrifugation and washed with water, dried, and used in the new cycle. Fig. 15 shows that the catalytic performance of both nanocomposites (rGO-Ag-C and rGO-Ag-U) were decreased after five cycles. The decrease of catalytic efficiency might be related to the loss of the nanocomposites during the recovery process due to the small amount of the nanocomposites used in the reduction of 4-NP.

4. Conclusions

In summary, a facile and simple sonochemical method was developed for the synthesis of rGO-Ag nanocomposite without using any additional reactants or capping agents. Optimize the conditions indicated that the rGO-Ag-U was obtained in 10 min sonication at 70% amplitude under ambient conditions, while the rGO-Ag-C obtained by

heating the mixture at 150 °C for 3.5 h. The TEM images showed that the small Ag NPs (about 18 nm) with uniform distribution loaded on the surface of rGO nanosheets by ultrasound method. The catalytic reduction of 4-NP to 4-AP was also confirmed that the rGO-Ag-U has a highly catalytic performance (k_{app} = 1.18 min^{-1}) compared with the rGO-Ag-C (k_{app} = 0.18 min^{-1}). The significant difference in catalytic activity between two nanocomposites can be related to the difference of Ag NPs size on the rGO surface. It was hypothesized that the rGO nanosheets played important roles in the catalytic properties of rGO-Ag nanocomposite: 1) the prevention of the Ag NPs agglomeration and aiding to growth of small nanoparticles with high surface area, 2) the increase of adsorption of the 4-NP molecules by π-π stacking interactions, 3) the raise of electron transfer rate from donor (BH_4^-) to acceptor electron (4-NP) via extended π-conjugation structure.

Acknowledgment

The support of Ferdowsi University of Mashhad (Research and Technology) Iran, for this work (code 3/42720, date 4/12/2016) is appreciated.

References

[1] V. Georgakilas, J.A. Perman, J. Tucek, R. Zboril, Broad family of carbon nanoallotropes: classification, chemistry, and applications of fullerenes, carbon dots, nanotubes, graphene, nanodiamonds, and combined superstructures, Chem. Rev. 115 (2015) 4744–4822.
[2] D.P. Hansora, N.G. Shimpi, S. Mishra, Graphite to graphene via graphene oxide: an overview on synthesis, properties, and applications, JOM 67 (2015) 2855–2868.
[3] S. Bykkam, V.R. Kalagadda, B. Kalagadda, K.P. Selvam, Y. Hayashi, Ultrasonic-assisted synthesis of ZnO nano particles decked with few layered graphene nanocomposite as photoanode in dye-sensitized solar cell, J. Mater. Sci. Mater. Electron. 28 (2017) 6217–6225.
[4] A. Esmaeili, M.H. Entezari, Cubic Ag/AgBr-graphene oxide nanocomposite: sonosynthesis and use as a solar photocatalyst for the degradation of DCF as a pharmaceutical pollutant, RSC Adv. 5 (2015) 97027–97035.
[5] E. Velez-fort, C. Mathieu, E. Pallecchi, M. Pigneur, M.G. Silly, R. Belkhou, M. Marangolo, A. Shukla, F. Sirotti, A. Ouerghi, M. Curie, Y. Cedex, Epitaxial graphene on 4H-SiC (0001) grown under nitrogen flux : evidence of low nitrogen doping and high charge transfer, ACS Nano 6 (2012) 10893–10900.
[6] A. Esmaeili, M.H. Entezari, Facile and fast synthesis of graphene oxide nanosheets via bath ultrasonic irradiation, J. Colloid Interface Sci. 432 (2014) 19–25.
[7] C. Higashi, Y. Funasaki, H. Iguchi, T. Maruyama, In situ polymerization of a novel surfactant on a graphene surface for the stable dispersion of graphene in water, RSC Adv. 6 (2016) 88244–88247.
[8] S. Zhang, D. Zhang, X. Zhang, D. Shang, Z. Xue, D. Shan, X.-Q. Lu, Ultratrace naked-eye colorimetric detection of Hg^{2+} in wastewater and serum utilizing mercury-stimulated peroxidase mimetic activity of reduced graphene oxide-PEI-Pd nanohybrids, Anal. Chem. 89 (2017) acs.analchem.6b04805.
[9] T. Gunji, S.H. Noh, T. Tanabe, B. Han, C.Y. Nien, T. Ohsaka, F. Matsumoto, Enhanced electrocatalytic activity of carbon-supported ordered intermetallic palladium-lead (Pd3Pb) nanoparticles toward electrooxidation of formic acid, Chem. Mater. 29 (2017) 2906–2913.
[10] R. Bhandari, M.R. Knecht, Isolation of template effects that control the structure and function of nonspherical, biotemplated pd nanomaterials, Langmuir 28 (2012) 8110–8119.
[11] M. Pelaez, N.T. Nolan, S.C. Pillai, M.K. Seery, P. Falaras, A.G. Kontos, P.S.M. Dunlop, J.W.J. Hamilton, J.A. Byrne, K. O'Shea, M.H. Entezari, D.D. Dionysiou, A review on the visible light active titanium dioxide photocatalysts for environmental applications, Appl. Catal. B Environ. 125 (2012) 331–349.
[12] M.-Q. Yang, X. Pan, N. Zhang, Y.-J. Xu, A facile one-step way to anchor noble metal (Au, Ag, Pd) nanoparticles on a reduced graphene oxide mat with catalytic activity for selective reduction of nitroaromatic compounds, CrystEngComm 15 (2013) 6819.
[13] R. Fenger, E. Fertitta, H. Kirmse, A.F. Thünemann, K. Rademann, Size dependent catalysis with CTAB-stabilized gold nanoparticles, Phys. Chem. Chem. Phys. 14 (2012) 9343.
[14] C. Cui, Y. Wang, D. Liang, W. Cui, H. Hu, B. Lu, S. Xu, X. Li, C. Wang, Y. Yang, Photo-assisted synthesis of Ag_3PO_4/reduced graphene oxide/Ag heterostructure photocatalyst with enhanced photocatalytic activity and stability under visible light, Appl. Catal. B Environ. 158–159 (2014) 150–160.
[15] S. Dutta, C. Ray, S. Sarkar, M. Pradhan, Y. Negishi, T. Pal, Silver nanoparticle decorated reduced graphene oxide (rGO) nanosheet: a platform for SERS based low-level detection of uranyl ion, ACS Appl. Mater. Interfaces. 5 (2013) 8724–8732.
[16] H. He, C. Gao, Supraparamagnetic, conductive, and processable multifunctional graphene nanosheets coated with high-density Fe_3O_4 nanoparticles, ACS Appl. Mater. Interfaces. 2 (2010) 3201–3210.
[17] Y. Li, W. Gao, L. Ci, C. Wang, P.M. Ajayan, Catalytic performance of Pt nanoparticles on reduced graphene oxide for methanol electro-oxidation, Carbon N. Y. 48 (2010) 1124–1130.
[18] J. Tian, S. Liu, Y. Zhang, H. Li, L. Wang, Y. Luo, A.M. Asiri, A.O. Al-Youbi, X. Sun, Environmentally friendly, one-pot synthesis of Ag nanoparticle-decorated reduced graphene oxide composites and their application to photocurrent generation, Inorg. Chem. 51 (2012) 4742–4746.
[19] K. Vinodgopal, B. Neppolian, I.V. Lightcap, F. Grieser, M. Ashokkumar, P.V. Kamat, Sonolytic design of graphene-Au nanocomposites. simultaneous and sequential reduction of graphene oxide and Au(III), J. Phys. Chem. Lett. 1 (2010) 1987–1993.
[20] B. Neppolian, C. Wang, M. Ashokkumar, Sonochemically synthesized mono and bimetallic Au-Ag reduced graphene oxide based nanocomposites with enhanced catalytic activity, Ultrason. Sonochem. 21 (2014) 1948–1953.
[21] A.M. Golsheikh, H.N. Lim, R. Zakaria, N.M. Huang, Sonochemical synthesis of reduced graphene oxide uniformly decorated with hierarchical ZnS nanospheres and its enhanced photocatalytic activities, RSC Adv. 5 (2015) 12726–12735.
[22] K. Vinodgopal, B. Neppolian, N. Salleh, I.V. Lightcap, F. Grieser, M. Ashokkumar, T.T. Ding, P.V. Kamat, Dual-frequency ultrasound for designing two dimensional catalyst surface : Reduced graphene oxide – Pt composite, Colloids Surfaces A Physicochem. Eng. Asp. 409 (2012) 81–87.
[23] W. Shen, Y. Qu, X. Pei, S. Li, S. You, J. Wang, Z. Zhang, J. Zhou, Catalytic reduction of 4-nitrophenol using gold nanoparticles biosynthesized by cell-free extracts of Aspergillus sp. WL-Au, J. Hazard. Mater. 321 (2017) 299–306.
[24] P. Zhao, X. Feng, D. Huang, G. Yang, D. Astruc, Basic concepts and recent advances in nitrophenol reduction by gold-and other transition metal nanoparticles, Coord. Chem. Rev. 287 (2015) 114–136.
[25] S. Ibrahim, S. Chakrabarty, S. Ghosh, T. Pal, Reduced graphene oxide – zinc sulfide composite for solar light responsive photo current generation and photocatalytic 4-nitrophenol reduction, ChemistrySelect 2 (2017) 537–545.
[26] J. Wu, W. Liu, X. Xiang, K. Sun, F. Liu, C. Cai, S. Han, Y. Xie, S. Li, X. Zu, From Ni$(OH)_2$/Graphene composite to Ni@Graphene core-shell: a self-catalyzed epitaxial growth and enhanced activity for nitrophenol reduction, Carbon N. Y. 117 (2017) 192–200.
[27] D.C. Marcano, D.V. Kosynkin, J.M. Berlin, A. Sinitskii, Z. Sun, A. Slesarev, L.B. Alemany, W. Lu, J.M. Tour, Improved synthesis of graphene oxide, ACS Nano 4 (2010) 4806–4814.
[28] J. Shen, M. Shi, N. Li, B. Yan, H. Ma, Y. Hu, M. Ye, Facile synthesis and application of Ag-chemically converted graphene nanocomposite, Nano Res. 3 (2010) 339–349.
[29] S.P. Dubey, M. Lahtinen, M. Sillanpää, Tansy fruit mediated greener synthesis of silver and gold nanoparticles, Process Biochem. 45 (2010) 1065–1071.
[30] S. Gurunathan, K. Kalishwaralal, R. Vaidyanathan, D. Venkataraman, S.R.K. Pandian, J. Muniyandi, N. Hariharan, S.H. Eom, Biosynthesis, purification and characterization of silver nanoparticles using Escherichia coli, Colloids Surfaces B Biointerfaces 74 (2009) 328–335.
[31] T. Sakai, H. Enomoto, K. Torigoe, H. Sakai, M. Abe, Surfactant- and reducer-free synthesis of gold nanoparticles in aqueous solutions, Colloids Surfaces A Physicochem. Eng. Asp. 347 (2009) 18–26.
[32] X. Wang, L. Shao, W. Guo, J. Wang, Y. Zhu, C. Wang, Ultrasonics Sonochemistry Synthesis of dendritic silver nanostructures by means of ultrasonic irradiation, Ultrason. Sonochem. 16 (2009) 747–751.
[33] C. He, L. Liu, Z. Fang, J. Li, J. Guo, J. Wei, Formation and characterization of silver nanoparticles in aqueous solution via ultrasonic irradiation, Ultrason. Sonochem. 21 (2014) 542–548.
[34] B. Neppolian, A. Doronila, F. Grieser, Simple and efficient sonochemical method for the oxidation of arsenic (III) to arsenic (V), Environ. Sci. Technol. 43 (2009) 6793–6798.
[35] J.E. Park, M. Atobe, T. Fuchigami, Synthesis of multiple shapes of gold nanoparticles with controlled sizes in aqueous solution using ultrasound, Ultrason. Sonochem. 13 (2006) 237–241.
[36] M. Govarthanan, T. Selvankumar, K. Manoharan, R. Rathika, K. Shanthi, K.J. Lee, M. Cho, S. Kamala-Kannan, B.T. Oh, Biosynthesis and characterization of silver nanoparticles using Panchakavya, an Indian traditional farming formulating agent, Int. J. Nanomed. 9 (2014) 1593–1599.
[37] G. Chen, Symbiosis theory-directed green synthesis of silver nanoparticles and their application in infected wound healing, Int. J. Nanomed. 11 (2016) 2757–2767.
[38] T. Yang, H.Y. Zou, C.Z. Huang, Synergetic catalytic effect of $Cu_{2-x}Se$ nanoparticles and reduced graphene oxide coembedded in electrospun nanofibers for the reduction of a typical refractory organic compound, ACS Appl. Mater. Interfaces. 7 (2015) 15447–15457.
[39] Y. Zuo, J.-M. Song, H.-L. Niu, C.-J. Mao, S.-Y. Zhang, Y.-H. Shen, Synthesis of TiO_2-loaded $Co_{0.85}$ Se thin films with heterostructure and their enhanced catalytic activity for p-nitrophenol reduction and hydrazine hydrate decomposition, Nanotechnology 27 (2016) 145701.
[40] W. Ye, J. Yu, Y. Zhou, D. Gao, D. Wang, C. Wang, D. Xue, Green synthesis of Pt-Au dendrimer-like nanoparticles supported on polydopamine-functionalized graphene and their high performance toward 4-nitrophenol reduction, Appl. Catal. B Environ. 181 (2016) 371–378.
[41] L. Liu, R. Chen, W. Liu, J. Wu, D. Gao, Catalytic reduction of 4-nitrophenol over Ni-Pd nanodimers supported on nitrogen-doped reduced graphene oxide, J. Hazard. Mater. 320 (2016) 96–104.
[42] J. Sun, Y. Fu, G. He, X. Sun, X. Wang, Catalytic hydrogenation of nitrophenols and nitrotoluenes over a palladium/graphene nanocomposite, Catal. Sci. Technol. 4 (2014) 1742.
[43] M. Kohantorabi, M.R. Gholami, Kinetic analysis of the reduction of 4-nitrophenol catalyzed by CeO_2 nanorods-supported CuNi nanoparticles, Ind. Eng. Chem. Res. 56 (2017) 1159–1167.
[44] M. Sharma, A. Mishra, A. Mehta, D. Choudhury, S. Basu, Enhanced catalytic and antibacterial activity of nanocasted mesoporous silver monoliths: kinetic and thermodynamic studies, J. Sol-Gel Sci. Technol. 81 (2017) 704–710.
[45] S. Saha, A. Pal, S. Kundu, S. Basu, T. Pal, Photochemical green synthesis of calcium-alginate-stabilized Ag and Au nanoparticles and their catalytic application to 4-nitrophenol reduction, Langmuir 26 (2010) 5920–5928.